J Mater Sci (2011) 46:6140–6147
DOI 10.1007/s10853-011-5579-4

Effects of particle plasticity characteristics on local interface stress in particle reinforced composite during uniaxial tension

H. M. Xu · G. Q. Wu · W. Sha

Received: 12 December 2010 / Accepted: 19 April 2011 / Published online: 5 May 2011

Abstract For elastoplastic particle reinforced metal matrix composites, failure may originate from interface debonding between the particles and the matrix, both elastoplastic and matrix fracture near the interface. To calculate the stress and strain distribution in these regions, a single reinforcing particle axisymmetric unit cell model is used in this article. The nodes at the interface of the particle and the matrix are tied. The development of interfacial decohesion is not modelled. Finite element modelling is used, to reveal the effects of particle strain hardening rate, yield stress and elastic modulus on the interfacial traction vector (or stress vector), interface deformation and the stress distribution within the unit cell, when the composite is under uniaxial tension. The results show that the stress distribution and the interface deformation are sensitive to the strain hardening rate and the yield stress of the particle. With increasing particle strain hardening rate and yield stress, the interfacial traction vector and internal stress distribution vary in larger ranges, the maximum interfacial traction vector and the maximum internal stress both increase, while the interface deformation decreases. In contrast, the particle elastic modulus has little effect on the interfacial traction vector, internal stress and interface deformation.

H. M. Xu · G. Q. Wu (✉)
School of Materials Science and Engineering,
Beihang University, Beijing 100083, China
e-mail: guoqingwu@buaa.edu.cn

W. Sha
School of Planning, Architecture and Civil Engineering,
Queen's University Belfast, Belfast BT7 1NN, UK

Introduction

Particle reinforced metal matrix composites have high specific strength, specific modulus and wear resistance and high temperature capability. They have received wide attention from aeronautical, space, automotive, mechanical and electronic fields. A good understanding of the mechanical behaviour of particle reinforced metal matrix composites will help improve materials design and processing. Researchers started studying these since 1980s [1–6]. Fracture of particle reinforced metal matrix composites mainly appears as debonding between particles and the matrix, ductile fracture in the matrix near the interface and fracture of reinforcing particles. Therefore, it is very important to study the mechanical behaviour in the proximity of the particles. During studying the local mechanical behaviour of this type of composites, there are difficulties in experimental design and mathematical complexity in theoretical derivation. For these reasons, computer simulation using the finite element method is widely used.

In computer simulation of these materials, an axisymmetric unit cell model containing a single reinforcing particle is often used. This model assumes that the unit cell contains only one reinforcing particle, in the centre of the symmetrical axis of the unit cell. According to periodical conditions, the unit cell should have a hexagonal shape. In practice, however, for simplifying analysis, the hexagonal shape is often reduced to cylinder. The particle shapes are usually approximated using simple geometrical shapes, for examples, spherical, spheroidal and cylindrical. Because this model can be simplified to two-dimensional, it uses a small number of finite elements, facilitating fast computation. It has attracted wide adoption [1, 7].

In the past, when using computer simulation with the finite element method, usually, the reinforcing particles are

assumed to the linear elastic. There is a general perception that adding elastic and hard particles in composites strengthens the material [8, 9], while adding ductile particles toughens the material [10]. There is much work on toughening using rubber particles [11]. In practice, different material properties must be considered together. There is soft adhesion of particles on matrix in elastoplastic particle reinforced metal matrix composites, which can improve the local stress distribution in the material. This has attracted attention. YAl_2 particle reinforced Mg–Li matrix composite was developed in [12], with superior properties. However, there has not been literature report on numerical simulation of local stresses in elastoplastic particle reinforced metal matrix composites. This article will carry out such simulation using the single reinforcing particle axisymmetrical unit cell model. Considering the local damage mode of the material, the nodes at the interface of the particle and the matrix are tied. Assuming that reinforcing particles are elastoplastic, we will study the effects of particle strain hardening rate, yield strength and elastic modulus on the mechanical behaviour within the unit cell.

The computer model and material parameters

The axisymmetric unit cell model containing a single reinforcing particle is shown in Fig. 1. Its geometrical configuration is shown in Fig. 2. The particle is spherical. Figure 2 shows a quarter of the unit cell model, where AFE is part of the particle and FBCDE is part of the matrix. The radius of the spherical particle is $10a_0$. The matrix has a cylindrical shape, and its radius is $20a_0$. The height of the cylinder is $40a_0$, which can be deduced from Fig. 2. Correspondingly, the volume fraction of particle V_f is 1/12, i.e. the quotient of the particle volume and the whole cell. During model setting up, due to symmetry, the three-dimensional unit cell was simplified to two-dimensional. The deformable two-dimensional solid structure was used, and it is in the symmetrical model space. The symmetrical axis is the AD side. In model meshing, four-node bilinear symmetrical quadrilateral elements were used. The element type is axisymmetric solid.

The nodes at the interface of the particle and the matrix are tied. In this manuscript, the interface is supposed to have zero thickness. The particle is stuck on the matrix, and the nodes at the interface of the particle and the matrix are fixed together. The nodes at the interface of the particle and the matrix are tied. The Young's modulus of the matrix and the particle is 76 and 460 GPa, respectively. The Poisson's ratio of the matrix and the particle is 0.33 and 0.25, respectively. The development of interfacial decohesion is not modelled. As shown in Fig. 2, this assumes a thin layer

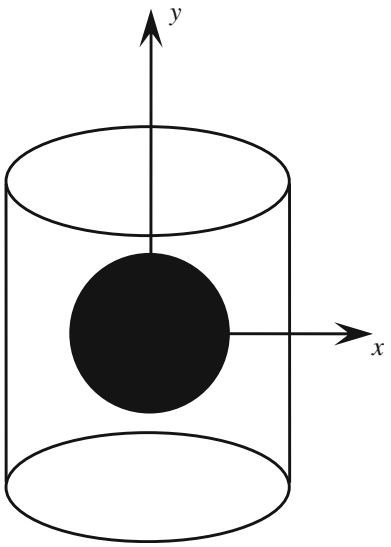

Fig. 1 Schematic diagram of axisymmetric unit cell model containing a single reinforcing particle

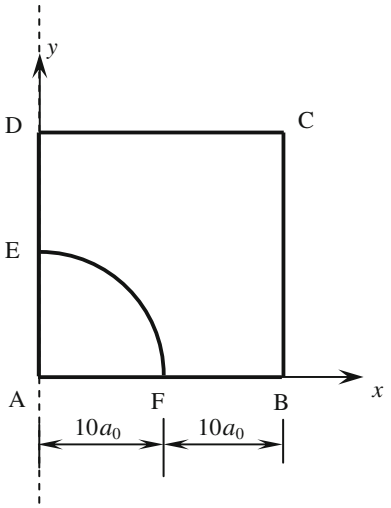

Fig. 2 Schematic diagram of the geometrical configuration of the unit cell and the interface model

on the interface, which connects the particle and the matrix, ensuring the continuity of the interfacial traction vector between the particle and the matrix and the continuity of displacement.

The stress–strain curves of reinforcing elastoplastic particles and the matrix are shown in Fig. 3. Aluminium alloy is used as the matrix material. A piecewise function used by Xue et al. [13] was adopted to describe its stress–strain relationship:

$$\sigma = \begin{cases} E_{\mathrm{Al}}\varepsilon & \varepsilon \le \sigma_{\mathrm{s1}}/E_{\mathrm{Al}} \\ 464\varepsilon^{0.136}(\mathrm{MPa}) & \varepsilon > \sigma_{\mathrm{s1}}/E_{\mathrm{Al}} \end{cases} \quad (1)$$

where E_{Al} is the elastic modulus of the aluminium alloy, σ_{s1} is the yield strength of the aluminium alloy. A linear

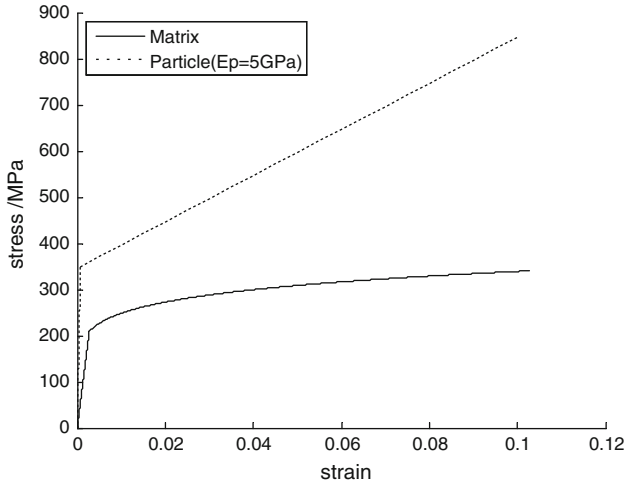

Fig. 3 Stress–strain curves of the elastoplastic particle and the matrix

hardening elastoplastic model is used to describe the particle, with its stress–strain relationship as follows:

$$\sigma = \begin{cases} E\varepsilon & \sigma \le \sigma_s \\ \sigma_s + E_p\varepsilon_p & \sigma > \sigma_s \end{cases} \quad (2)$$

where E is the elastic modulus of the particle material, σ_s is its yield strength, E_p is its strain hardening rate, ε_p is its plastic strain, which has a relationship with the total strain $\varepsilon_p = \varepsilon - \sigma_s/E$. The linear hardening model is intended to correspond to a sort of strengthen materials, not any specific material, say, YAl_2, and the matrix material is a kind of Al alloy.

The bulk particle reinforced composite is made up with many such small unit cells, packing repeatedly [1]. When the bulk material is under tension in the y-direction, for each unit, it may be assumed that there is no stress in the x-direction along the BC side, and the BC and DC sides remain straight (Fig. 2). In order to achieve these conditions, after applying a displacement of $2a_0$ of DC in y-direction, a trial displacement of x_0a_0 is applied on the BC side along the x-direction, to enable the following condition along the BC side:

$$\sum_{i=1}^{n} \sigma_{11}^{i} = 0 \quad (3)$$

where n is the node number along the BC side, and the superscript i refers to the ith node. If the applied trial displacement cannot make the average stress in the x-direction along the BC side zero, i.e. Eq. 3 does not stand; a new trial value for x_0 is used, until Eq. 3 is satisfied. This is a gradually approaching process. When Eq. 3 is satisfied, the unit cell state is properly conditioned, to represent a part in the bulk material under uniaxial tension in the y-direction.

The material is composed of cells periodically distributed, and under the loading the deformation of the cell surfaces is uniform. The upper surface DC maintains a state of plane, which is easy to comprehend and realise through the displacement boundary conditions in the software. BC maintains a uniformly deformed curved surface around the same axis AD. All of the above determined the loading method.

In the simulation, the standard Abaqus (version 6.7) FE package software was used. The boundary conditions at faces AB and AD can be deduced from Figs. 1 and 2, i.e. AD is the axial symmetry axis and AB is an axis of symmetry of the plane ABCD. The unit of ABCD represent a circle of 360°, so the boundary condition of AB and AD is lateral symmetry and axial symmetry, respectively.

Alternatively, with displacement-based finite element algorithms the appropriate radial displacements of axisymmetric cells have usually been obtained by designating one node on face BC as a master node and slaving the radial displacements of all other nodes on this face (the "slave nodes") to this degree of freedom. Such an approach, on the one hand, does not require iterating (making it more efficient) and, on the other hand, does not explicitly require the nodal stress values at model surfaces, which tend to be inaccurate in displacement-based FE models. The boundary conditions used by the authors may therefore be considered unconventional.

The figures in the following ("The effect of particle strain hardening rate on the local stress at the interface", "The effect of particle yield strength on the local stress at the interface" and "The effect of particle elastic modulus on the local stress at the interface" sections) will show the effects of particle parameters. Among these, the first group of five figures ("The effect of particle strain hardening rate on the local stress at the interface" section) shows the effect of strain hardening rate of the particle on the interfacial traction vector and particle deformation. The second group of five figures ("The effect of particle yield strength on the local stress at the interface" section) shows the effect of particle yield strength and the third group of five figures ("The effect of particle elastic modulus on the local stress at the interface" section) shows the effect of particle elastic modulus. The material used in the second and the third groups ("The effect of particle yield strength on the local stress at the interface" and "The effect of particle elastic modulus on the local stress at the interface" sections) is ideal plastic. In all these figures, the value of the uniaxial macroscopic displacement of the DC side is $2a_0$. The direction of the profiles is with respect to the direction of $E \rightarrow F$. $\theta = 0$ corresponds to point E and $\theta = 90°$ corresponds to point F.

The effect of particle strain hardening rate on the local stress at the interface

It can be seen from Fig. 4 that, with increasing strain hardening rate of the particle, the variation of the normal component of the interfacial traction vector increases, and the maximum normal component of the interfacial traction vector increases. For an E_p of 460 GPa, i.e. when the particle is an elastic particle, the maximum tensile stress is 502 MPa, the maximum compressive stress is 128 MPa, which are at $\theta = 76.5°$ and $\theta = 9°$, respectively. When θ is smaller than 9°, with increasing θ, the compressive stress increases. When θ is in the range of 9° and 76.5°, with increasing θ, σ_N changes from compressive to tensile, and increases monotonously. When θ is greater than 76.5°, σ_N reduces gradually. For an E_p of zero, i.e. when the particle is ideal plastic, the maximum tensile stress is at $\theta = 90°$, about 348 MPa, and the minimum stress is zero, at $\theta = 0°$. When E_p changes from 0 to 460 GPa, the magnitude of the normal component of the interfacial traction vector σ_N becomes less sensitive to E_p when E_p is large. When E_p is larger than 100 GPa, there is no obvious influence of the change in E_p on σ_N. In general, the debonding between the particle and the matrix is mainly determined by the normal component of the interfacial traction vector between the particle and the matrix. From the above analysis, it can be inferred that, compared with elastic particles, plastic particles have a lower demand on the interfacial traction vector between the particle and the matrix. From Fig. 5, it can be seen that, with increasing strain hardening rate of the particle, the tangential component of the interfacial traction vector increases. When E_p is 460 GPa, i.e. elastic particle, the maximum value of the interfacial tangential stress occurs at $\theta = 40.5°$, about 259 MPa. When θ is smaller than 40.5°, with increasing θ, τ_N increases. When θ

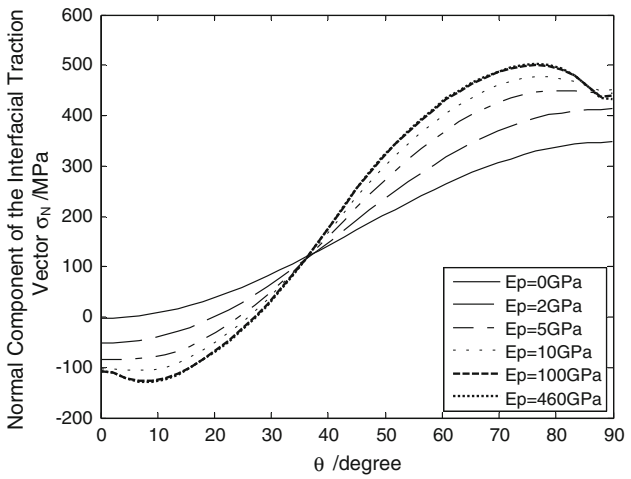

Fig. 4 The relationship between strain hardening rate E_p and the normal component of the interfacial traction vector

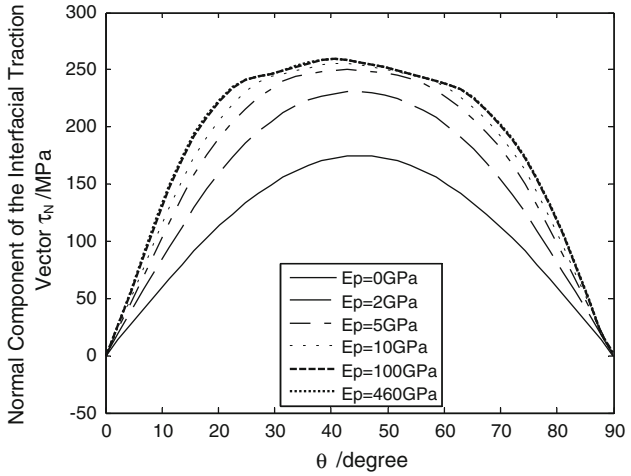

Fig. 5 The relationship between strain hardening rate E_p and the tangential component of the interfacial traction vector

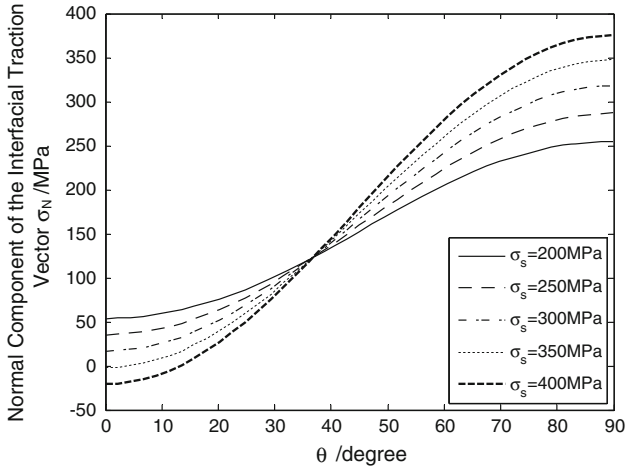

Fig. 6 The relationship between yield strength σ_s and the normal component of the interfacial traction vector

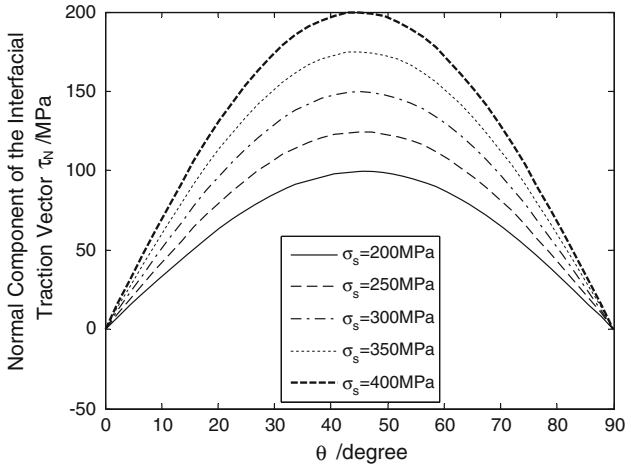

Fig. 7 The relationship between yield strength σ_s and the tangential component of the interfacial traction vector

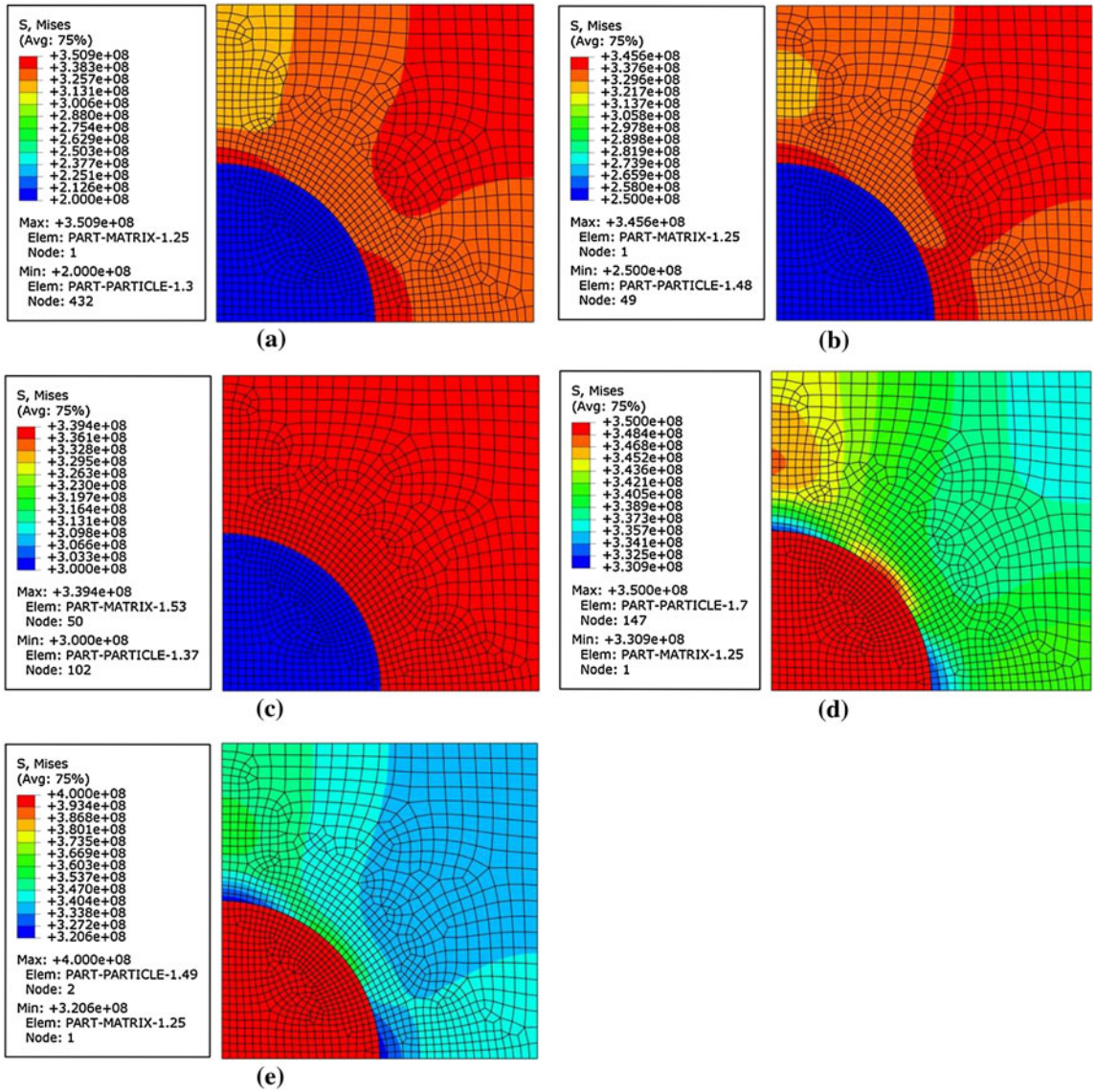

Fig. 8 Contour diagrams of Von Mises stress for different yield strength σ_s. **a** $\sigma_s = 200$ MPa, **b** $\sigma_s = 250$ MPa, **c** $\sigma_s = 300$ MPa, **d** $\sigma_s = 350$ MPa and **e** $\sigma_s = 400$ MPa

is greater than 40.5°, with increasing θ, τ_N decreases. τ_N is zero at $\theta = 0°$ and 90°. For zero E_p, i.e. ideal plastic particle, the maximum τ_N is about 175 MPa. For different E_p values, the variation in τ_N is 84 MPa. Therefore, the particle material being plastic, instead of elastic, also has a lower demand on the shear resistance of the interface, under uniaxial tension. The shear stress is more sensitive to E_p for smaller E_p. When E_p is greater than 100 MPa, E_p has little effect on τ_N.

It should be noted that the boundary condition used is displacement, and the applied stress is not a uniform one, so normalised stress values could not be obtained. The complex condition is due to the cell being periodically distributed part of the material.

The yielding amount can be qualitatively deduced from the figures.

The effect of particle yield strength on the local stress at the interface

The yield strength σ_s of the particle also influences interaction between the particle and the matrix at the interface. Figures 6 and 7 show the distributions of normal and tangential components of the interfacial traction vector.

As can be seen in Fig. 6, increasing σ_s leads to wider ranges of variation of the normal component of the interfacial traction vector (σ_N). When σ_s is 400 MPa, the lower limit

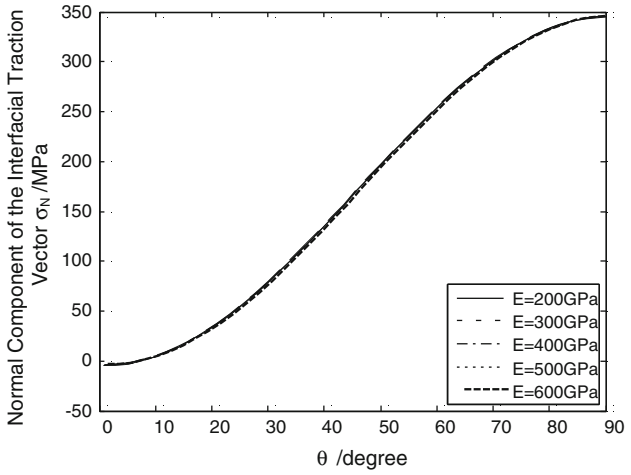

Fig. 9 The relationship between the particle's elastic modulus E and the normal component of the interfacial traction vector

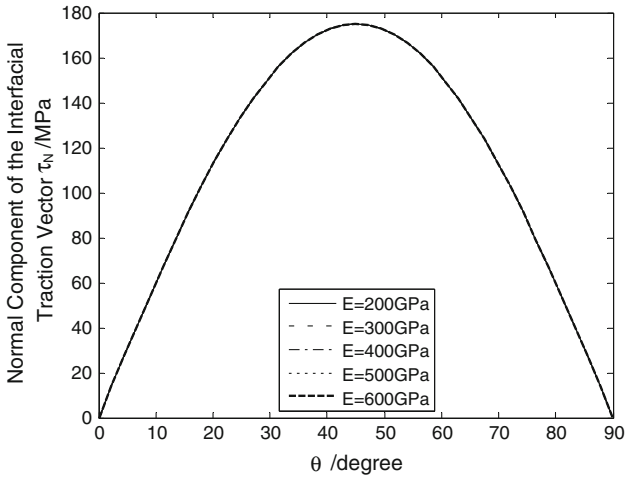

Fig. 10 The relationship between the particle's elastic modulus E and the tangential component of the interfacial traction vector

of σ_N at the interface is compressive, −20 MPa, while the upper limit is tensile, 376 MPa. When σ_s is 200 MPa, however, the lower limit of σ_N at the interface is tensile, 53.8 MPa, while the upper limit is tensile, 255 MPa. In addition, it should be noted that, when σ_s is 200–300 MPa, the normal component of the interfacial traction vector is always tensile, but when σ_s is 350–400 MPa, the normal component of the interfacial traction vector changes from compressive at small θ to tensile as θ increases. This is because, when σ_s is $\leq$300 MPa, the Von Mises stress in the matrix is larger than the Von Mises stress in the particle, clearly shown in Fig. 8a–c. In addition, when σ_s is 350 MPa, the minimum normal component of the interfacial traction vector is around zero. This does not mean that $\sigma_s = 350$ MPa is a critical yield stress. This particular value is related to the vertical displacement applied, and thus is largely incidental. Finally, a small σ_s leads to smaller differences between the upper and the lower limits of the normal component of the interfacial traction vector, showing the advantage of using weaker particles. However, we cannot make the conclusion that, because small σ_s gives uniform interface stress distribution, we should choose a material with the smallest σ_s. In practical applications, small σ_s only indicates that debonding is less likely between the particle and the matrix. It may be detrimental to the overall properties. Therefore, in practice, its combined effect, both microscopically and macroscopically, must be analysed.

It can be seen in Fig. 7 that, with increasing σ_s, the maximum value of the tangential component of the interfacial traction vector increases, which always occurs at $\theta = 45°$. When σ_s is 400 MPa, $\tau_{N\max}$ is 200 MPa. When σ_s is 200 MPa, however, $\tau_{N\max}$ is 99 MPa, showing the advantage of weaker material. Second, along the interface, except at F point ($\theta = 0°$) and E point ($\theta = 90°$), increasing σ_s always leads to increasing τ_N. E and F points are not affected by the yield stress of the particle, and τ_N is zero for all values of σ_s. Finally, for any yield stress σ_s, τ_N exhibits a parabola type of variation. With increasing angle θ, τ_N first increases and then decreases. In materials design, τ_N on the interface at around $\theta = 45°$ should be given particular attention to.

From the above analysis of Figs. 6 and 7, a lower yield stress results in larger deformation of the particle. This not really surprising, provided that the applied load is sufficiently high for causing yielding of the particle.

For simplicity, the contours of the Von Mises stress of the composite on only the section of x–y plane are shown here, in Fig. 8. Under the boundary conditions specified, the particle reached its yield stress in all cases. In the matrix, when σ_s is smaller than 300 MPa, higher yield stress results in reductions of the maximum and the minimum Von Mises stresses. When σ_s is larger than 300 MPa, higher yield stress results in increases of the maximum and the minimum Von Mises stresses. This value of 300 MPa is determined by the boundary conditions in this calculation case, so its exact value is actually incidental. On the other hand, in the matrix, when σ_s is smaller than 300 MPa, the Von Mises stress adjacent to the particle interface does not vary significantly. When σ_s is larger than 300 MPa, the extreme values of the Von Mises stress on the particle interface differ more with increasing σ_s.

The effect of particle elastic modulus on the local stress at the interface

Figures 9 and 10 show the influence of particle elastic modulus on the interfacial traction vector. It can be seen that the effect of elastic modulus has a relatively small effect on the material. The distributions of σ_N and τ_N each

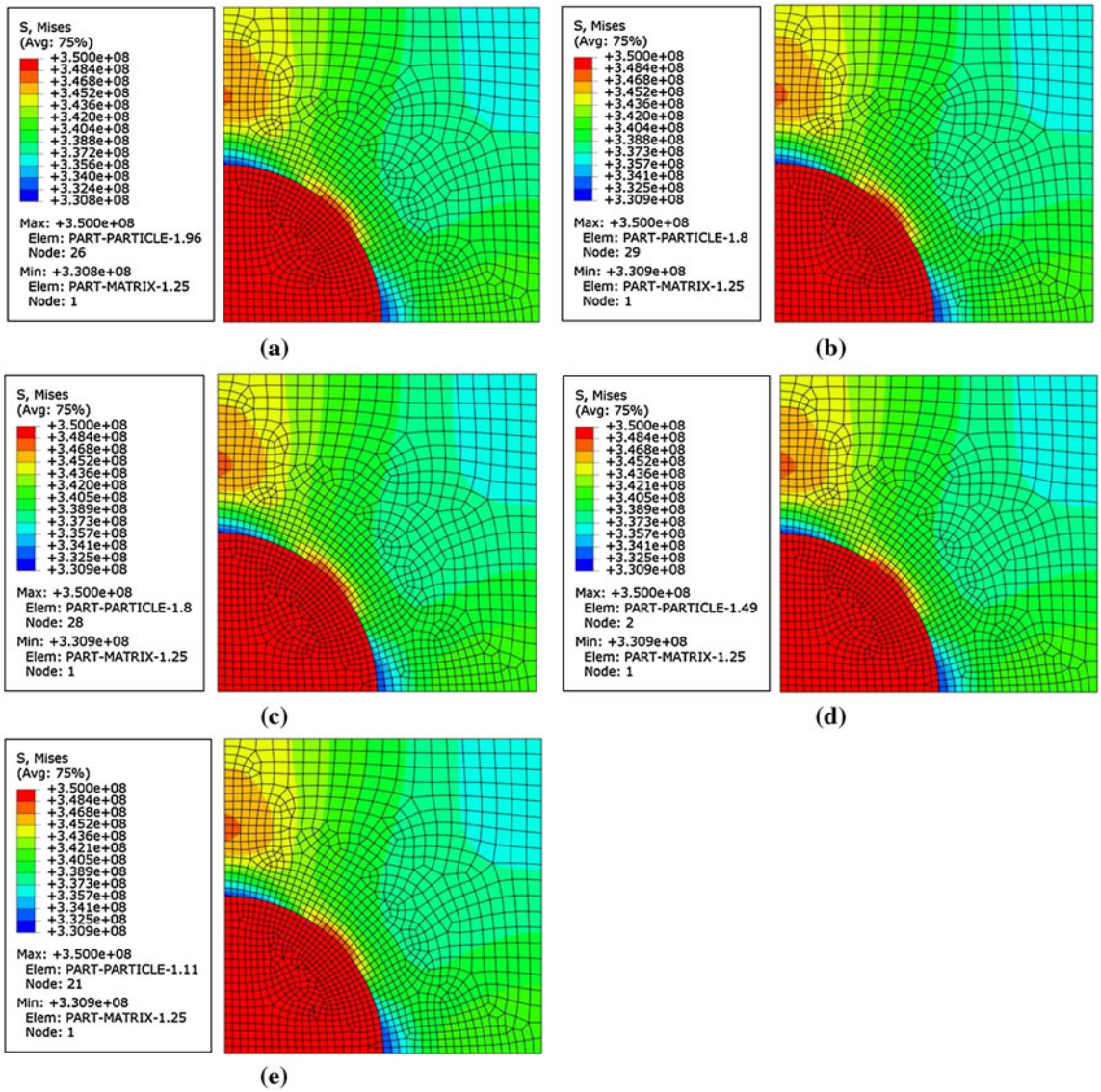

Fig. 11 Contour diagrams of Von Mises stress for different particle's elastic modulus E. **a** $E = 200$ GPa, **b** $E = 300$ MPa, **c** $E = 400$ GPa, **d** $E = 500$ MPa and **e** $E = 600$ GPa

overlaps the corresponding curves in Figs. 4 and 5 for $E_p = 0$. The calculation results here show that the elastic modulus has minute and negligible effect on these parameters.

In addition, from Fig. 11 showing the contour diagrams on the x–y section, there is virtually no influence of the particle elastic modulus on the distribution of Von Mises stress. A weak influence is in the exact location of the maximum Von Mises stress. Two regions, in the matrix right above the particle at a distance of about $5a_0$ and the interface between the particle and the matrix around 40–50°, respectively, have relatively large Von Mises stress. These areas should be given attention to during materials design.

Conclusion

An axisymmetric unit cell model containing a single reinforcing particle has been used, to simulate particle reinforced metal matrix composites using elastoplastic particles as reinforcements. Finite element modelling has been used, to analyse the effects of particle characteristics on the local stress near the interface in the composite, under uniaxial tension. Based on the simulation and analysis results, the following conclusions can be made:

(1) The stress distribution and the interface deformation are relatively sensitive to the strain hardening rate and the yield stress. In contrast, the change in the elastic

modulus has relatively little effect on the interface adhesion stress, internal stress and the interface deformation.

(2) Larger strain hardening rate and yield stress lead to larger variations in the interface adhesion stress and internal stress, resulting in larger maxima of these stresses. However, the interface deformation decreases.

Acknowledgements This research project is supported by the Ph.D. Programs Foundation of Ministry of Education of China (No. 20070006020), the Foundation of Beijing Technology New-Star (Nova) Program (No. 2007B016), and the National Natural Science Foundation of China (50901005).

References

1. Guild FJ, Young RJ (1989) J Mater Sci 24:298. doi:10.1007/BF00660971
2. Llorca J, Elices M, Termonia Y (2000) Acta Mater 48:4589
3. Segurado J, Llorca J, Gonzalez C (2002) Scr Mater 46:525
4. Segurado J, Llorca J (2002) J Mech Phys Solids 50:2017
5. Llorca J, Segurado J (2004) Mater Sci Eng A 365:267
6. Böhm HJ, Eckschlager A, Han W (2002) Comput Mater Sci 25:42
7. Han W, Eckschlager A, Böhm HJ (2001) Comp Sci Technol 61:1581
8. Sahu S, Broutman LJ (1972) Polym Eng Sci 12:91
9. Lu S, Yan L, Zhu X, Qi Z (1992) J Mater Sci 27:4633. doi:10.1007/BF01165998
10. Wu S (1987) Polym Eng Sci 27:335
11. Choi J, Yee AF, Laine RM (2004) Macromolecules 37:3267
12. Wang SJ, Wu GQ, Li RH, Luo GX, Huang Z (2006) Mater Lett 60:1863
13. Xue Z, Huang Y, Li M (2002) Acta Mater 50:149